High-temperature solution nitriding and low-temperature surface nitriding of 3D printed stainless steel

Valente, Emilie Hørdum; Christiansen, Thomas Lundin; Somers, Marcel A. J.

Publication date:
2018

Document Version
Peer reviewed version

High-temperature solution nitriding and low-temperature surface nitriding of 3D printed stainless steel

Emilie H. Valente, Thomas L. Christiansen, Marcel A. J. Somers

Technical University of Denmark, Department of Mechanical Engineering, Produktionstorvet b.425, 2800 Kgs. Lyngby, Denmark, {emhval, tch, somers}@mek.dtu.dk

Abstract

The present work focuses on gaseous thermochemical treatment of stainless steel parts produced by Selective Laser Melting (SLM). Specifically, high temperature solution nitriding (HTSN) and low temperature surface nitriding (LTSN) of SLM 316L stainless steel samples are investigated.

The cellular structure and the fusion-boundaries present in the as-printed SLM 316L stainless steel are removed by austenitisation and HTSN treatment. The treatments result in a homogenization of the printed microstructure and a lower bulk hardness compared to the as printed state. Due to the continued presence of elongated austenite grains, the removal of the cellular structure is attributed to recovery and/or elemental homogenisation. LTSN was performed successfully on SLM samples after both austenitisation and HTSN, resulting in a hardened layer consisting of expanded austenite. Pre-treatment with HTSN leads to a thicker case and higher hardness as compared to austenitisation as a pre-treatment.

Keywords

Selective laser melting, stainless steel, microstructure, gaseous nitriding

1 Introduction

In recent years, various processes for 3D printing of metal have been developed and commercialized [Frazier 2014], among which Selective Laser Melting (SLM). In SLM a laser is used to selectively (locally) melt and solidify the powder in a powder bed system, thus the 3D component is build layer by layer.

Due to the repetitive melting and heating of individual areas, vertical layer-by-layer building and extreme cooling rates, the microstructure of SLM produced metal parts is generally inhomogeneous and may contain non-equilibrium phases, which are responsible for anisotropic mechanical properties [Mertens 2014].

Recent characterisation of the hierarchical microstructure of SLM manufactured AISI 316L revealed an inhomogeneous microstructure, characterised by elongated austenite grains bridging over several fusion boundaries marking adjacent layers. Within the austenite grains a cellular structure was found, where the dislocation rich inter-cellular walls were small angle grain boundaries enriched in Mo and Cr [Wang et al. 2017].

One of the most critical challenges for 3D printed stainless steel parts is the poor corrosion resistance as compared to wrought counterparts of the same alloy. In general, this is attributed to the rough surface containing many crevices, porosity and the inherent inhomogeneous microstructure and chemical composition. The later was confirmed by Trelewicz et al. who investigated the influence of the SLM-printed microstructure of austenitic stainless steel 316L. They proposed that the reduced corrosion resistance was due to inhomogeneous solute distribution and inhomogeneous microstructures, leading to a lower quality of the passive layer.

Moreover, they observed a higher etch-resistance of the Mo-enriched inter-cellular walls [Trelewicz et al. 2016].

Gaseous nitriding of steel is a useful method to alter the microstructure in order to improve the properties of a material, such as strength, hardness, wear and/or corrosion resistance [Christiansen, Somers 2013, Bottoli et al. 2017]. The process of nitriding has been known and applied since the 1920s and numerous specialized treatments to tailor materials properties, as well as the development of specialty nitriding steels, have been developed over the years. For obvious reasons these treatments (and alloys) were developed for traditionally manufactured components, not for additive manufacturing such as 3D printing.

High temperature solution nitriding (HTSN) is a thermochemical process that is performed at temperatures beyond the dissolution temperature of Cr-based carbides or nitrides. Generally, a modest increase of the nitrogen content in combination with a case depth up to several millimeters are achieved. This process improves the yield strength while preserving the ductility of the steel. On the other hand, low-temperature surface hardening (LTSH) is a process that is performed at a temperature where Cr-based nitrides are stable but for kinetic reasons develop only after prolonged treatment (annealing). Generally, a high nitrogen content is obtained in combination with a shallow case depth (appr. 20–30 µm). The high nitrogen content is in supersaturated solid solution and significantly enhances the hardness by solid solution strengthening and work hardening as a consequence of the simultaneous plastic deformation introduced by the large lattice expansion. Apart from an important increase in hardness which improves the wear resistance also the localized corrosion, i.e. pitting and crevice corrosion, resistance is importantly improved by the dissolution of nitrogen.

The present work deals with HTSN and LTSN of SLM manufactures AISI 316 steel.

2 Experimental

SLM 316L samples were manufactured at the Danish Technological Institute (DTI), using stainless steel 316L powder (Ø10–45 µm) from SLM Solutions, with the composition provided in Table 1.

The samples were built in a MCP Realizer SLM 250, using the following parameters: 80 µm hatch distance, 50 µm layer thickness, 0.533 m/s laser speed (150 µs/80 µm) and 159 W laser power. The samples were printed in the geometry Ø10 x 10 mm cylinders, with a 3.5 mm wide and 7.5 mm deep centre hole for threads. The parts were built on support structures consisting of the same material, in a nitrogen atmosphere, using the antiparallel stripes scanning pattern, with the centre of the cylinder along the build direction as illustrated in Figure 1.

Element	**Fe**	**C**	**Si**	**Mn**	**P**	**S**	**Cr**	**Ni**	**Mo**	**N**
Minimum [wt%]	Bal.	-	-	-	-	-	16.00	10.00	2.00	-
Actual [wt%]	Bal.	0.030	0.59	0.85	0.12	0.004	17.6	12.8	2.32	0.09
Maximum [wt%]	Bal.	0.030	1.00	2.00	0.045	0.030	18.00	14.00	3.00	0.10

Table 1: Chemical composition of 316L powder, as provided by supplier SLM Solutions

All as printed samples were ground flat on the outer surfaces with P80 paper, followed by 30 seconds grinding with P220, P320, P500, P1000 and P4000 papers in order to obtain a well-defined surface condition for the subsequent thermal and thermochemical treatments. The SLM samples were investigated in the as-printed state (AP), after austenitisation (A), after high-temperature solution nitriding (HTSN), after austenitisation followed by low-temperature surface nitriding (LTSN) and after consecutive HTSN and LTSN.

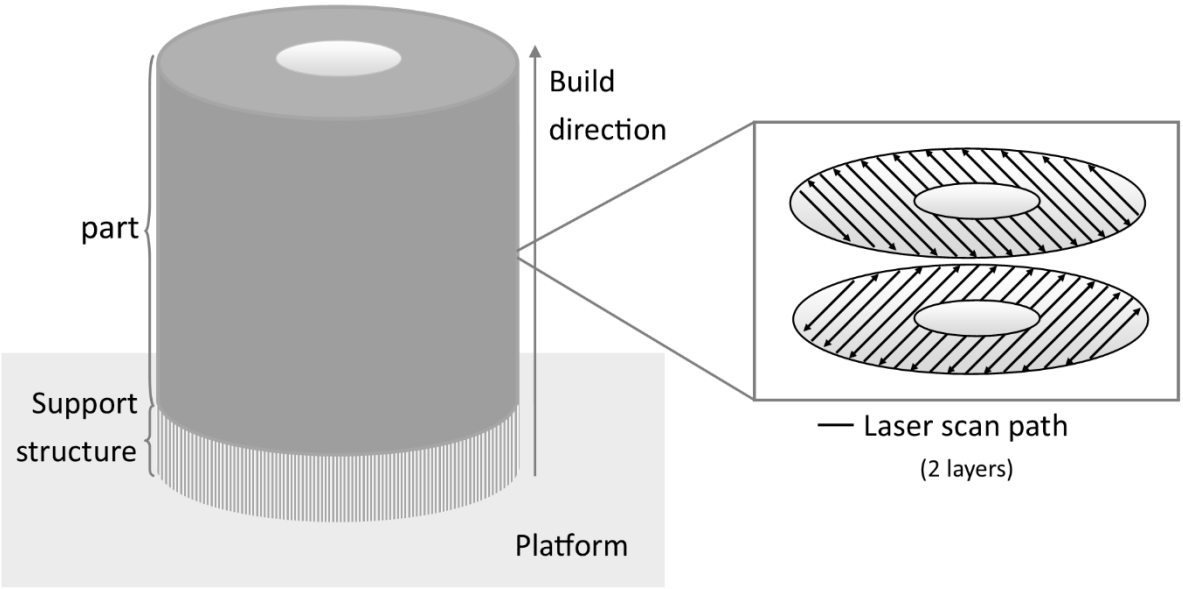

Figure 1: Illustration of part geometry, build direction and scan strategy

Austenitising was performed at 1353 K (1080 ˚C) for 10 minutes in a horizontal tube furnace, flushed with 500 ml/min high purity hydrogen and 100 ml/min high purity argon. High temperature solution nitriding was performed by Expanite A/S in accordance with their patented High-T treatment [Christiansen, Hummelshøj, Somers 2012, 2013]. Low-temperature surface nitriding was performed on austenitised samples and on HTSN-treated samples. The treatment was performed in a Netzsch STA449 F3 thermobalance, equipped with ammonia, hydrogen and argon gas flow. After proprietary in-situ activation the LTSN process was run at atmospheric pressure at 713 K (440 ˚C), in a two-stage (boost) nitriding treatment, consisting of 100 ml NH_3/min for 1 h, followed by 60 ml NH_3/min and 40 ml H_2/min for 15 h. For all treatments a flow of 5 ml Ar/min was applied.

Phase analysis of the as-printed, heat treated and thermochemically modified samples was performed using X-ray diffraction on a Bruker D8 Discovery equipped with Cr$K\alpha$ radiation. X-ray diffractograms in symmetrical $\theta - 2\theta$ scans in parallel beam geometry were recorded at a step size of 0.04 ˚2θ and a measurement time of 8 s per step. Cross-sections were prepared for investigation of microstructure and hardness, by cutting the samples along the centre, parallel to the build direction. The as-printed samples were etched in a solution containing 4 % HNO_3 and 1 % HF, for 18 minutes, while the treated samples were etched with Kallings no. 2 for 5–8 seconds. Special care was taken during preparation, due to the presence of porosities and during etching, as the poor corrosion resistance in the as-printed condition is reflected in strongly inhomogeneous etching behaviour. The microstructures were investigated with light optical microscopy and scanning electron microscopy (JEOL JSM-5900). Vickers micro-hardness indentations were carried out on a ground and polished cross-section, using a Struers DuroScan 70-G5 micro-hardness. For the LTSN samples a FM-700 micro-hardness tester was used to measure along 1 µm grid profiles in the hardened case. All hardness measurements were performed with a load of 10 g and a dwell time of 10 s.

3 Results & interpretation

3.1 As-printed condition

The microstructure of the SLM printed 316L was investigated with reflected light microscopy, revealing a hierarchical microstructure of elongated γ austenite grains with a fine cellular

structure, shown in Figure 2. The presence of both spherical gas porosities and incomplete melting pores was observed in the cross-sections.

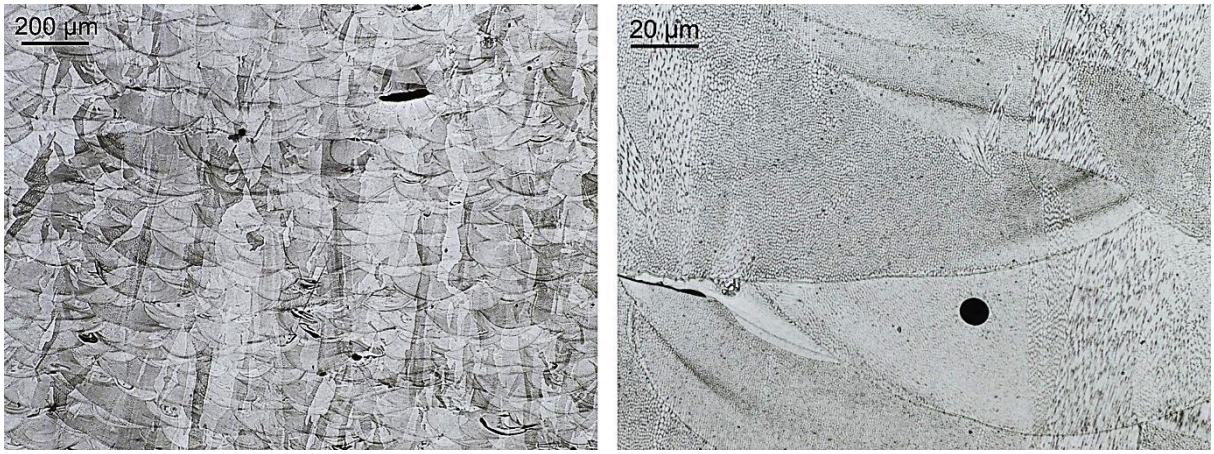

Figure 2: Light optical micrographs of the as-printed SLM 316L samples, showing elongated γ austenite grains (left) and a cellular structure and fusion-boundaries (right). Etched for 18 minutes in a 4 % HNO_3 and 1 % HF solution.

The microstructure was further investigated with scanning electron microscopy (SEM), shown in Figure 3, were the fusion-boundaries are marked with arrows (see Figure 3 (left)). The cellular structure changes at the austenite grain boundaries and occasionally at the fusion-boundaries, e.g. the fusion-boundary shown in Figure 3 (right), where three different austenite grains are visible. Two austenite grains are visible to the left and evidenced by different directions of the cellular structure on each side of the fusion-boundary, i.e. a high angle grain boundary. The cellular structure in the austenite grain to the right does not change size and direction, and continues over the fusion-boundary. The high magnification SEM micrograph (Figure 3 (right)) reveals how the fusion-boundary is heavily attacked by the etchant, while the cellular walls are less affected, thus indicating a higher concentration of the elements Mo and Cr at the cellular walls; this is consistent with literature (cf. Introduction). The etching has also revealed the presence of small particles at the cellular walls (see Figure 3 (right)).

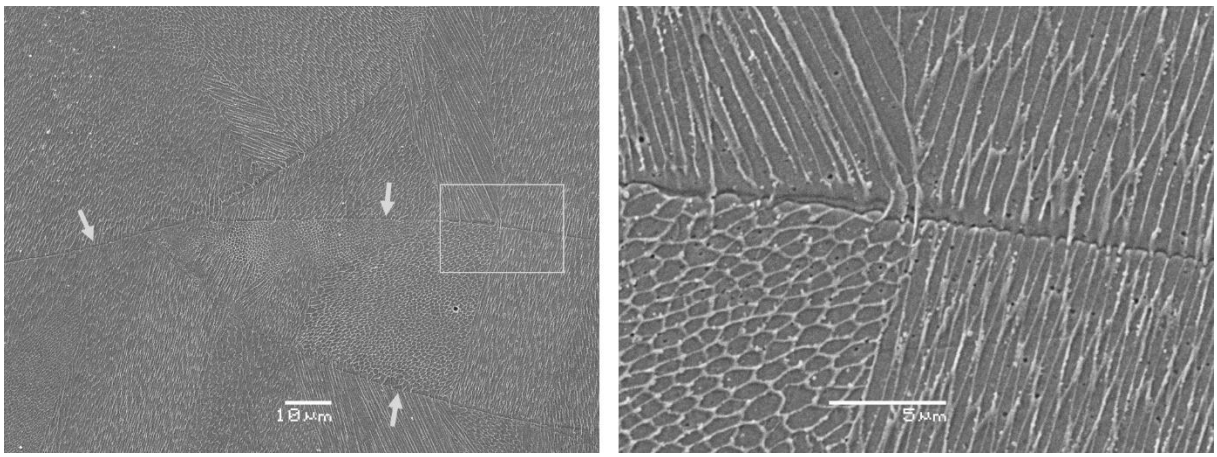

Figure 3: Secondary electron micrographs of the as-printed SLM 316L samples, showing the inhomogeneous microstructure, with arrows marking the fusion-boundaries (left) and a higher magnification of the cellular structure (right), from a scan at the area marked by the square (left). Etched for 18 minutes in a 4 % HNO_3 and 1 % HF solution.

The results of X-ray diffraction analysis are presented in Table 2 and Figure 4 and confirm the presence of a mainly austenitic structure in the as printed material (Figure 4 (top)). A small amount of δ-ferrite phase was also identified. The presence of δ-ferrite is a remnant of the

solidification during printing. Clearly, the as-printed condition shows peak broadening as compared to the austenitised condition (see Figure 3 (top) and Table 2).

sample	**a [nm]**	**FWHM [°2θ]**	
		111	200
as printed	0.35935	0.167	0.305
austenitised	0.35957	0.090	0.128
HTSN	0.36084	0.118	0.154

Table 2: Lattice parameter, a, and peak width, FWHM, as determined from austenite $K_{\alpha 1}$ reflections

The (asymmetric) broadening of the austenite peaks in the as-printed condition is attributed to the presence of the cellular structure (see Figure 2 (right) and 3). Both the chemical inhomogeneity (higher Cr and Mo content on the cell boundaries) and the enhanced dislocation density at the boundary are anticipated to contribute to broadening. The dimensions of the cells are beyond the threshold for quantifiable size broadening (approximately 200 nm), as the diameters are around 1 µm.

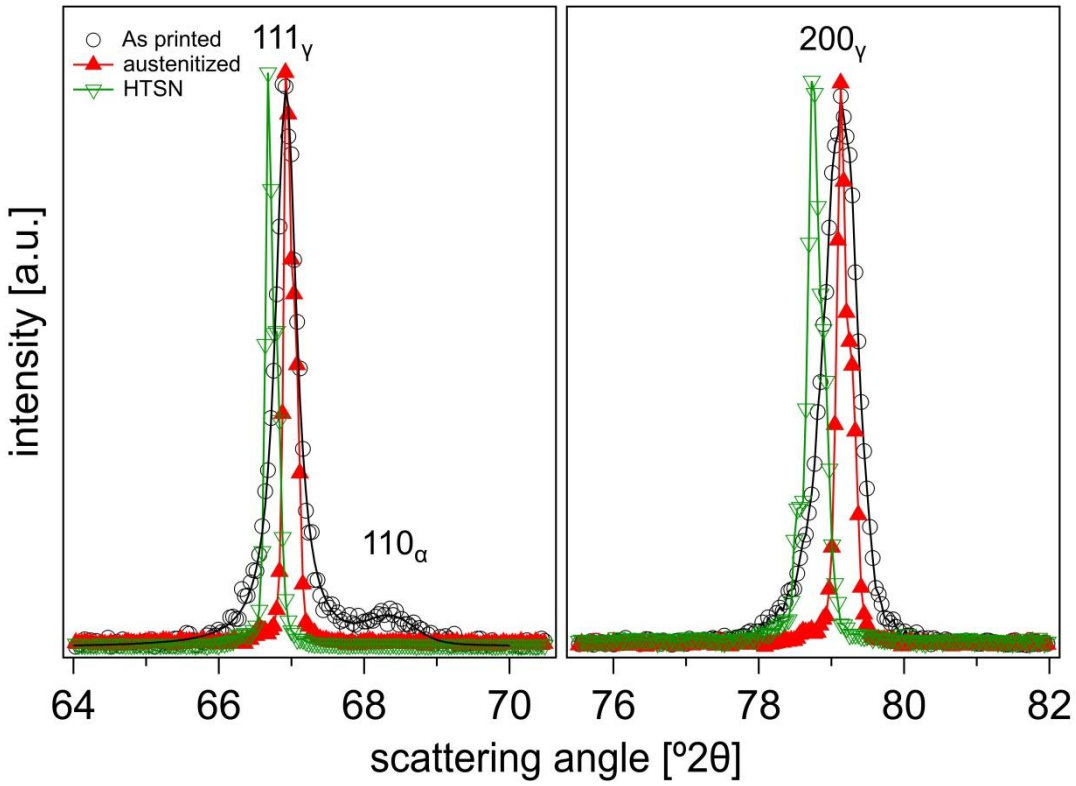

Figure 4: X-ray diffractograms of SLM 316L samples, showing the effect of austenitising and HTSN on the position and width of 111 and 200 austenite reflections. The intensities were normalized, such that the peaks can be straightforwardly compared.

3.2 High-temperature treatments

Etching of the austenitised samples revealed that the cellular structure, the fusion boundaries and δ-ferrite had disappeared (see Figures 4 and 5), leading to the abovementioned narrowing of the austenite peaks in X-ray diffractograms. The HTSN treatment leads to a shift of the austenite peaks to smaller Bragg angles (Figure 4) as a consequence of the dissolution of nitrogen in austenite and the associated modest expansion of the lattice. The minor broadening as compared

to the austenitised condition (Table 2) is most likely associated with fluctuations in the nitrogen content in the analysed volume. In the micrograph of the austenitised and the high-temperature solution nitrided samples (Figure 5), elongated austenite grains are clear for both treatments. For the austenitised sample, a wavy substructure, corresponding to remnants from the fusion-boundaries is visible, while this was not visible in the HTSN sample, indicating the higher temperature and longer treatment time of a HTSN treatment lead to further homogenisation of the microstructure as compared to the austenitisation treatment.

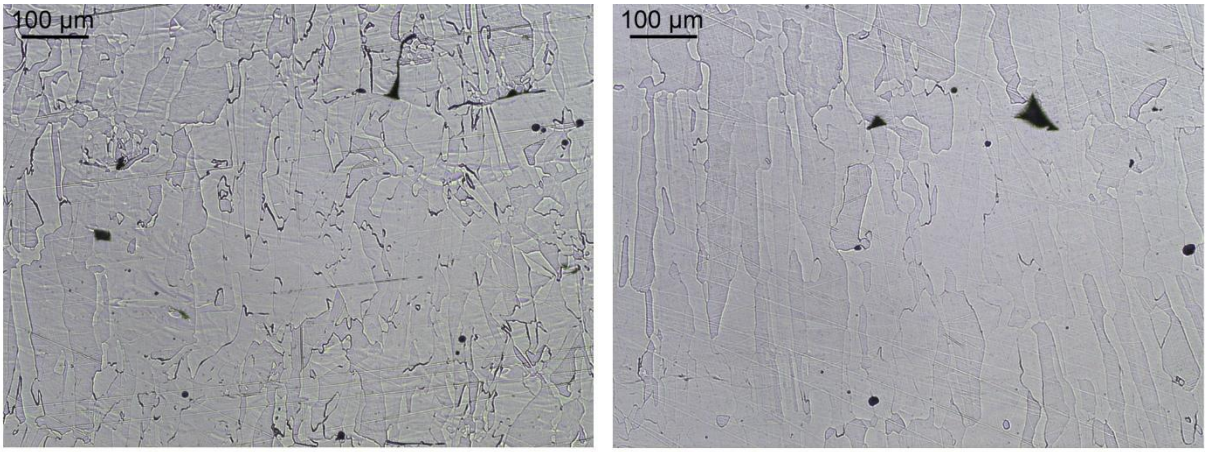

Figure 5: Light optical micrographs of SLM samples subjected to high temperature treatments. Etched for 8 seconds with Kallings, showing elongated γ austenite grains, and the presence of weak substructures in the austenitised samples which are remnants of the fusion-boundaries. The HTSN sample does not contain any substructures.

The hardness-depth profile after HTSN is shown in Figure 6. A hardness increase associated with the dissolution of nitrogen is observed to a depth of approximately 0.4 mm. For comparison also the average hardness values measured in the as printed and austenitised condition are provided in Figure 6. Not surprisingly, the dissolution of the cellular structure is associated with a reduction in hardness. As compared to 10 min austenitisation the HTSN gives a further reduction in hardness in the core of the sample.

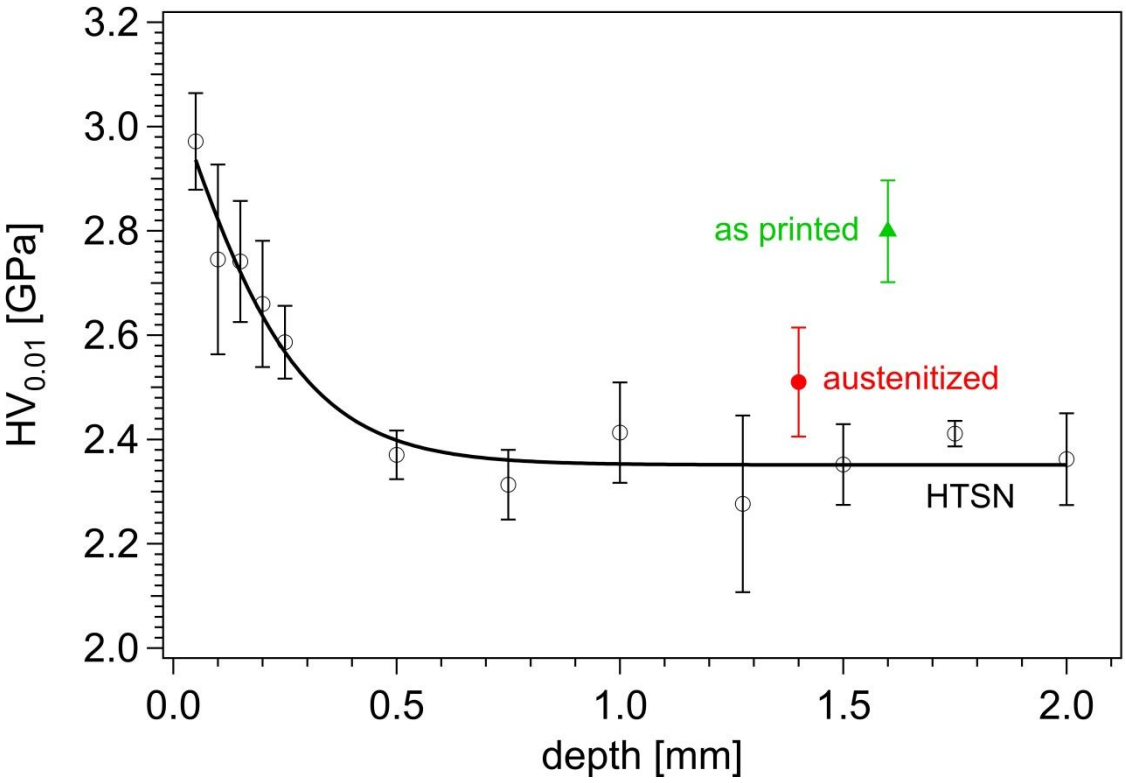

Figure 6: Micro-hardness profiles for the as-printed, austenitised and HTSN samples. Values represented by open markers are the average of at least 5 measurements and the error bar represent the standard deviation; the closed symbols represent the average over about 20 data points over a 2 mm depth range.

The slight difference in hardness between austenitised and HTSN (core) samples is not a consequence of grain growth, because the load applied during hardness indentation is so low that it is not affected by the size of the grains. Instead, the hardness decrease can be explained by the higher HTSN temperature and longer duration, which led to further homogenisation, observed with reflected light microscopy (Figure 5), and most likely also dissolution of microstructural features that remain undetected by the applied methods. The continued presence of the elongated austenite grains and the disappearance of the δ-ferrite peak in the patterns from both samples, indicates that only recovery and/or elemental homogenisation facilitated the removal of the cellular structure and the fusion boundaries.

3.3 Low-temperature surface nitriding

The low-temperature surface nitriding treatment was preceded by austenitisation or HTSN treatment. The resulting microstructures are shown in Figure 7 and reveal the presence of a zone of expanded austenite adjacent to the surface.

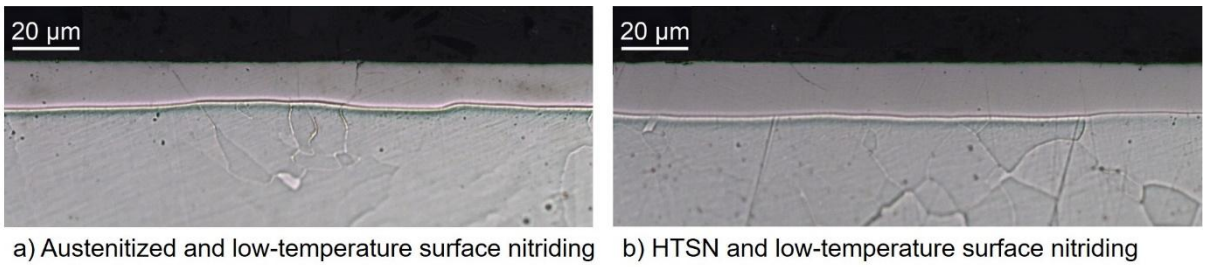

Figure 7: Light optical micrographs of SLM samples subjected to low-temperature surface nitriding (LTSN). Etched for 5 seconds with Kallings, showing the expanded austenite zones.

The corresponding X-ray diffractograms are presented in Figure 8 and confirm the presence of strong expanded austenite peaks, indicated as γ_N. The peaks are shifted to lower 2θ angles as compared to the austenite peaks as a consequence of the influence of lattice expansion by dissolving nitrogen in supersaturated solid solution and the associated compressive residual stresses. The shifts for 111 and 200 peaks are very different as a consequence of the elastic and plastic anisotropy, which leads to an appreciably larger shift for the elastically softer 100 direction (cf. Brink et al. 2017). The excessive broadening of the expanded austenite peaks is associated with the (steep) nitrogen concentration gradient and partially plastic accommodation of the lattice expansion, which introduced dislocations and lattice rotation. The diffractograms also show that for the LTSN treatment following an HTSN treatment, the austenite substrate peaks have disappeared, while they are still visible for the LTSN after austenitisation treatment. This is consistent with the thicker expanded austenite zone on the HTSN+LTSN sample (cf. Figure 7 and 9).

After low-temperature surface nitriding the hardness is substantially enhanced in the expanded austenite zone (Figure 9). The deeper expanded austenite zone on the HTSN+LTSN treated sample is explained from faster growth, which is determined from the difference in flux entering the surface and the flux leaving the expanded austenite zone into the steel. The nitrogen flux that leaves the expanded austenite zone and diffuses into the underlying austenite is reduced after HTSN, because nitrogen is already present. Hence, faster growth of the expanded austenite zone can occur.

In general, the present results show that HTSN and LTSN are possible on SLM produced 316L steel. The short austenitisation of 10 minutes at 1080 ˚C was enough to remove the cellular structure, but as observed in the micrograph and by the hardness, some inhomogeneity remains. Still, the austenitisation, leading to the removal of δ-ferrite and the cellular structures, should increase the corrosion resistance significantly, and preliminary polarization tests (not included) have shown both an increase in corrosion potential and pitting potential, and a highly improved passivation behaviour, compared to as-printed 316L. One could argue that austenitisation is a necessity on SLM produced 316L in order to get the corrosion performance associated with 316L stainless steel.

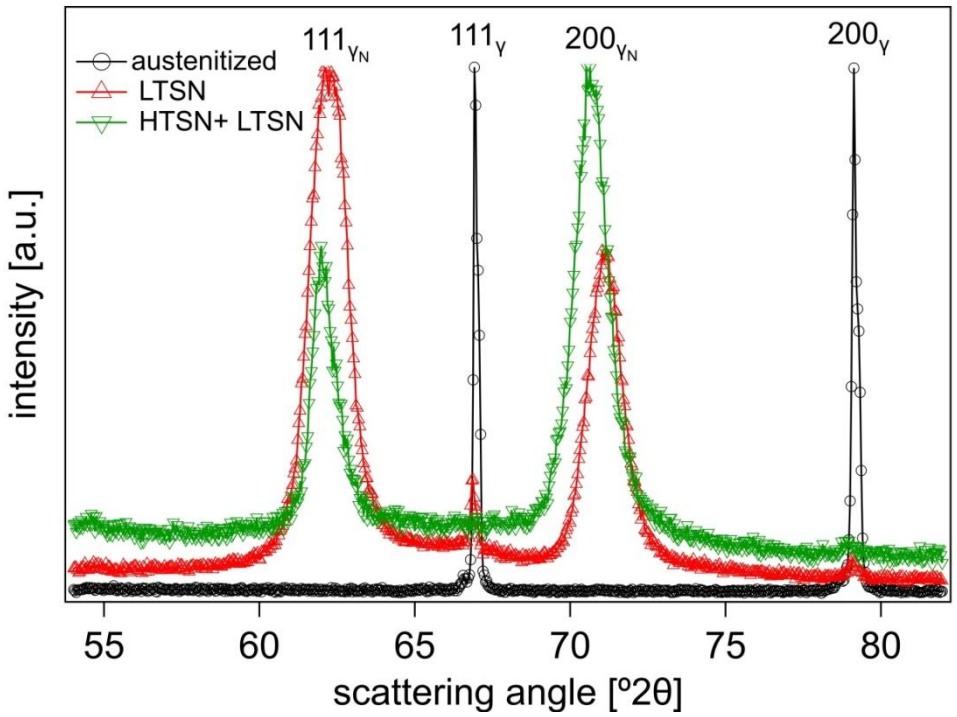

Figure 8: X-ray diffractograms of SLM 316L samples, showing the effect of LTSN after austenitising and after HTSN. The diffractogram for the austenitised samples is given as a reference. The intensities were normalized, such that the peaks can be straightforwardly compared.

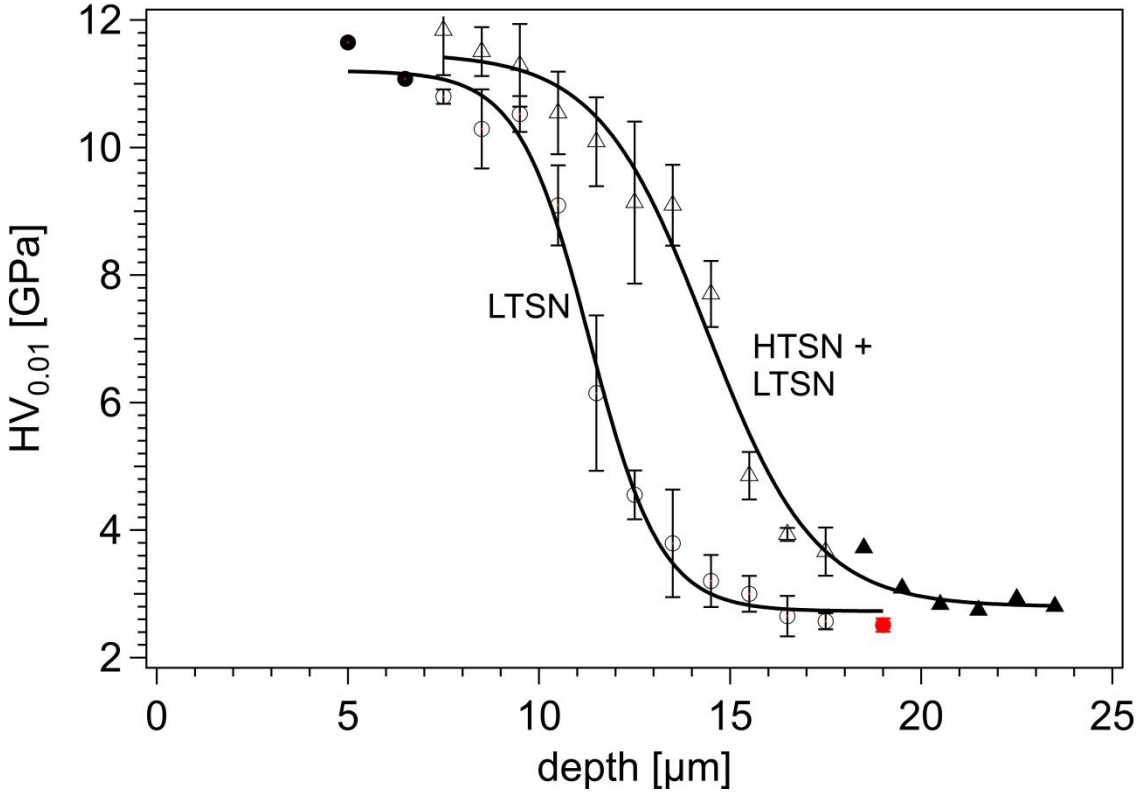

Figure 9: Micro-hardness profiles of the LTSN samples, showing the difference in the hardened layer close to the surface. Values represented by open markers are the average of at least 5 measurements and the error bar represent the standard variation; the closed symbols represent single datapoints.

The increased homogenisation observed in the HTSN samples, due to the longer duration and higher temperature, is expected to provide a further improvement in the corrosion properties. Secondly, nitrogen introduced by HTSN has been demonstrated to enhance the pitting potential [Bottoli et al. 2018], and the corrosion resistance is therefore expected to be improved significantly by HTSN as compared to the improvement obtained with austenitisation.

The additional LTSN treatment, was proven to increase the hardness in the surface, and is expected to appreciably increase both pitting and crevice corrosion resistance [Bottoli et al. 2018] and could therefore be considered as an option when both corrosion and wear properties need to be improved.

4 Conclusion

The hierarchical microstructure of 3D printed stainless steel AISI 316L is strongly heterogeneous and contains elongated austenite grains, remnants of δ-ferrite and a cellular structure related to the repeated fusion and solidification inherent to the 3D printing manufacturing. The cellular structure disappears on austenitisation and leads to a lowering of the hardness. High-temperature solution nitriding (HTSN) slightly enhances the hardness at the surface, because of the dissolution of nitrogen, and increases the homogenisation of the bulk microstructure, leading to a slight hardness decrease, compared to austenitisation. Low-temperature solution nitriding (LTSN) after austenitisation or after HTSN provides a hard surface zone of expanded austenite. The zone grows faster on a previously HTSN treated sample than after austenitising.

Acknowledgement

The authors wish to acknowledge the Danish Technological Institute for providing SLM samples.

References

Bottoli, F.; Jellesen, M. S.; Christiansen, T. L.; Winther, G.; Somers, M. A. J.: High temperature solution-nitriding and low-temperature nitriding of AISI 316: Effect on pitting potential and crevice corrosion performance. *Appl. Surf. Sci.*, vol. 431, pp. 24-31, 2018.

Brink, B.; Staåhl, K.; Oddershede, J.; Christiansen, T.L.; Winther, G.; Somers, M.A.J.: On the elusive crystal structure of expanded austenite, *Scr. Mater.*, vol. 113, pp. 59-62, 2017.

Christiansen, T.L.; Hummelshøj, T.S.; Somers, M.A.J: Forming Expanded Austenite and/or Expanded Martensite by Solution Hardening of Cold Deformed Workpiece of Passive Alloy, WO 146254-A1, 2012.

Christiansen, T.L.; Hummelshøj, T.S.; Somers, M.A.J: Solution Hardening of Cold Deformed Passive Alloy Workpiece Used to Form Component e.g. Lock Washer, Involves Dissolving Nitrogen in Workpiece and Cooling in Presence of Inert Gas Which Does Not Contain Nitrogen at Preset Temperature, WO2013159781-A1, 2013.

Christiansen, T. L.; Somers, M. A. J.: HTPro: Low-temperature Surface Hardening of Stainless Steel, *Adv. Mater. Process.* 52–53, 2013.

Frazier, W. E.: Metal additive manufacturing: A review, *Journal of Materials Engineering and Performance*, vol. 23, no. 6. Springer US, pp. 1917–1928, 2014.

Mertens, A. *et al.*: Mechanical properties of alloy Ti–6Al–4V and of stainless steel 316L processed by selective laser melting: influence of out-of-equilibrium microstructures, *Powder Metall.*, vol. 57, no. 3, pp. 184–189, 2014.

Trelewicz, J. R.; Halada, G. P.; Donaldson, O. K.; Manogharan, G.: Microstructure and Corrosion Resistance of Laser Additively Manufactured 316L Stainless Steel, J*om*, vol. 68, no. 3, pp. 850–859, 2016.

Wang, Y. M. *et al.*: Additively manufactured hierarchical stainless steels with high strength and ductility, *Nat. Mater.*, no. October, pp. 1–11, 2017.